Astron. Astrophys. 360, 583–591 (2000)

ASTRONOMY AND ASTROPHYSICS

A study of the dipping low mass X-ray binary X 1624-490 from the broadband BeppoSAX observation

M. Bałucińska-Church[1], **P.J. Humphrey**[1], **M.J. Church**[1], **and A.N. Parmar**[2]

[1] School of Physics and Astronomy, University of Birmingham, Birmingham B15 2TT, UK (mbc@star.sr.bham.ac.uk)
[2] Astrophysics Division, Space Science Department of ESA, ESTEC Postbus 299, 2200 AG Noordwijk, The Netherlands (aparmar@astro.estec.esa.nl)

Received 28 February 2000 / Accepted 24 May 2000

Abstract. We present results of a study of the luminous dipping low mass X-ray binary X 1624-490 made using *BeppoSAX*. An interval of deep and rapidly varying dipping was included in the observation. The radial intensity profile of the source obtained using the MECS instruments revealed excesses in intensity above the instrument point spread function below ∼5 keV demonstrating the presence of a dust-scattering halo. From modelling of the radial profile in several energy bands, halo intensity fractions rising to 30% in the lowest band 2.5–3.5 keV were obtained. From these data, the optical depth to dust scattering at 1 keV was found to be 2.4 ± 0.4. The non-dip spectrum of X 1624-490 in the energy band 1–100 keV is shown to be well-described by the emission model consisting of point-like blackbody radiation assumed to be from the neutron star plus extended Comptonized emission from an ADC. The blackbody temperature was 1.31 ± 0.07 keV and the Comptonized emission had photon power law index $2.0^{+0.5}_{-0.7}$ and cut-off energy ∼12 keV. The spectra of several dip levels were shown to contain an unabsorbed component below 5 keV. Good fits to the dip spectra were obtained by allowing the Comptonized emission to be progressively covered by an extended absorber while the blackbody was rapidly absorbed and a constant halo component accounted for dust scattering into the line-of-sight. It is shown that the unabsorbed component consists of the uncovered part of the Comptonized emission plus a halo contribution which in deepest dipping dominates the spectrum below 4.5 keV. From the dip ingress time, we have derived a diameter of the extended Comptonized emission region of $5.3 \pm 0.8 \times 10^{10}$ cm, consistent with a hot, X-ray emitting corona extending to ∼50% of the accretion disk radius. The source luminosity for a distance of 15 kpc is 7.3×10^{37} erg s^{-1}, an appreciable fraction of the Eddington limit making X 1624-490 the most luminous dipping LMXB. The half-height of the blackbody emitting region on the neutron star of 6.8 ± 1.8 km agrees with the half-height of the radiatively supported inner accretion disk of 6.3 ± 2.9 km, which together with similar agreement recently obtained for 13 other LMXB strongly supports the identification of the neutron star as the origin of the blackbody emission in LMXB. Finally, from *RXTE* ASM data, we derive an improved orbital period of 20.87±0.01 hr.

Key words: X-rays: stars – stars: individual: X 1624-490 – stars: neutron – stars: binaries: close – accretion, accretion disks – ISM: dust, extinction

1. Introduction

X 1624-490 is one of the most unusual members of the class of dipping Low Mass X-ray Binary (LMXB) sources exhibiting periodic dips in X-ray intensity. It is generally accepted that dipping is due to absorption in the bulge in the outer accretion disk where the accretion flow from the companion inpacts (White & Swank 1982). X 1624-490 has the longest orbital period of the dipping sources at 21±2 hr (Watson et al. 1985), but the period has not been refined since this determination from *Exosat*. Dipping is deep, ∼ 75% in the band 1–10 keV, and the source also exhibits strong flaring in which the X-ray flux can increase by 30% over timescales of a few thousand seconds (Church & Bałucińska-Church 1995).

The depth, duration and spectral evolution in dipping vary considerably from source to source. However, spectral analysis of dipping sources provides information not available in non-dip sources. For example, spectral models are more strongly constrained by having to fit non-dip and dip data, thus showing clearly the nature of the emission. In addition, the dip ingress and egress times can be used to obtain the sizes of the extended emission regions when the absorber has larger angular extent than the source regions, thus providing information on the geometry of the accretion disk corona (ADC) (e.g. Church et al. 1997). Although the fundamental question of the nature of the emission regions in LMXB is controversial, a unifying model has been proposed for the dipping class (Church & Bałucińska-Church 1995) which is able to explain the widely disparate behaviour of individual sources. The emission regions consist of the point source neutron star producing blackbody emission, and an extended Comptonizing region, probably the ADC. It has now been shown that this model not only can explain well the spectra of *all* dipping LMXB (Church et al. in prepara-

Send offprint requests to: M. Bałucińska-Church

tion), but can also explain the spectra of all the Z-track and Atoll sources investigated in a recent *ASCA* survey (Church & Bałucińska-Church 2000). In a number of dipping sources, the nature of dipping was not understood because of the clear presence of an unabsorbed part of the non-dip spectrum at all levels of dipping. In these sources, dip spectra could be modelled by dividing the non-dip spectral form into two parts: one absorbed and the other unabsorbed but with strongly decreasing normalization (Parmar et al. 1986; Courvoisier et al. 1986; Smale et al. 1992), 'absorbed plus unabsorbed' modelling. It has been difficult however, to explain these normalization changes convincingly. More recently, an alternative explanation has been suggested in which an extended absorber moves across the extended and point-like emission regions, providing a natural explanation for the unabsorbed component as the uncovered emission which becomes smaller as dipping proceeds. This Progressive Covering model has explained spectral evolution during dipping in XB 1916-053, XB 0748-676 and XB 1323-619 (Church et al. 1997, 1998a,b; Bałucińska-Church et al. 1999).

X 1624-490 was previously observed in a long *Exosat* observation of 220 ks and with *Ginga* (Jones & Watson 1989). The *Exosat* ME data revealed an apparently stable lower level of dipping supporting the presence of two emission components, one of which was totally absorbed in deep dipping. A blackbody plus bremsstrahlung model was used to parameterize the spectra (Jones & Watson 1989). Church & Bałucińska-Church (1995; hereafter CBC95) showed that the light curve at higher energies (> 5 keV) was dominated by flaring which can strongly modify the spectrum and make the spectral investigation of dipping difficult. By selecting sections of non-dip and dip data without apparent flaring, the above unifying blackbody plus Comptonization model was found to fit the data well showing that in deep dipping the blackbody component was totally absorbed, and that the Comptonized component was relatively little absorbed. However, with only one non-dip and one deep dip spectrum it was not possible to determine the extent of absorption of the Comptonized component. The Galactic column density of X 1624-490 is very high $\sim 8 \times 10^{22}$ atom cm^{-2} so that a dust scattered halo of the source is expected, and Angelini et al. (1997) demonstrated an excess of the surface brightness above the point spread function in *ASCA* GIS.

In the present paper, we present a detailed study of dipping in X 1624-490 and of the effects of dust scattering in this source made using *BeppoSAX*. With the very broad band, we have been able for the first time to obtain reliably parameters of the Comptonized emission. We also present a determination of the orbital period of X 1624-490 from the *RXTE* ASM.

2. Observations

Data from the Low-Energy Concentrator Spectrometer (LECS; 0.1–10 keV; Parmar et al. 1997), Medium-Energy Concentrator Spectrometer (MECS; 1.3–10 keV; Boella et al. 1997), High Pressure Gas Scintillation Proportional Counter (HPGSPC; 5–120 keV; Manzo et al. 1997) and the Phoswich Detection System (PDS; 15–300 keV; Frontera et al. 1997) on-board *BeppoSAX* are presented. All these instruments are coaligned and collectively referred to as the Narrow Field Instruments, or NFI. The MECS consists of three identical grazing incidence telescopes with imaging gas scintillation proportional counters in their focal planes, however prior to the observation of X 1624-490 one of the detectors had failed. The LECS uses an identical concentrator system as the MECS, but utilizes an ultra-thin entrance window and a driftless configuration to extend the low-energy response to 0.1 keV. The non-imaging HPGSPC consists of a single unit with a collimator that is alternatively rocked on- and off-source to monitor the background spectrum. The non-imaging PDS consists of four independent units arranged in pairs each having a separate collimator. Each collimator can be alternatively rocked on- and off-source to monitor the background.

The region of sky containing X 1624-490 was observed by *BeppoSAX* between 1998 August 11 00:47 and August 11 18:22 UTC. Good data were selected from intervals when the elevation angle above the Earth's limb was $>4^\circ$ for LECS and MECS, $>5^\circ$ for the HPGSPC and $>10^\circ$ for the PDS and when the instrument configurations were nominal, using the SAXDAS 1.3.0 data analysis package. The standard collimator dwell time of 96 s for each on- and off-source position was used, together with rocking angles of $180'$ and $210'$ for the HPGSPC and PDS, respectively. The exposures in the LECS, MECS, HPGSPC, and PDS instruments are 16 ks, 34 ks, 17 ks, and 16 ks, respectively. LECS and MECS data were extracted centered on the position of X 1624-490 using radii of $8'$ and $4'$. Background subtraction in the imaging instruments was performed using standard files scaled appropriately to match the background level in the image, this being required because of the location of the source in the Galactic plane, but is not critical for such a bright source. Background subtraction in the non-imaging instruments was carried out using data from the offset intervals.

3. Results

3.1. The X-ray lightcurve

Fig. 1 shows the background-subtracted MECS lightcurves of X 1624-490 with a binning of 32 s in two energy bands: 1.8–5.0 keV and 5.0–10.0 keV. Observation of dipping is difficult in this source with a long orbital period if the total observation time is to be kept within limits. In this case the observation was carried out on the basis of a dipping ephemeris we obtained from the *RXTE* ASM, aiming for the dipping to occur at the centre of the observation. Dipping was detected as seen in Fig. 1, lasting between 3.6 and 8.4 ks with parts being missed in data gaps. The total count rate was $\sim$11 count s^{-1}. Data in the high energy band reveal little flaring which was clearly seen in the *Exosat* ME as increases in count rate above 5 keV lasting several thousand seconds (CBC95), except for an increase in count rate of 20% at $\sim$32 ks lasting 1.4 ks. We detected little effect in the spectral fitting that might be due to flaring. An expanded view of the dipping in the band 1.8–10 keV is shown in Fig. 2 revealing strong variability on timescales of $\sim$32 s proving "blobbiness" in the absorber. Dips are not strongly evident in the HPGSPC

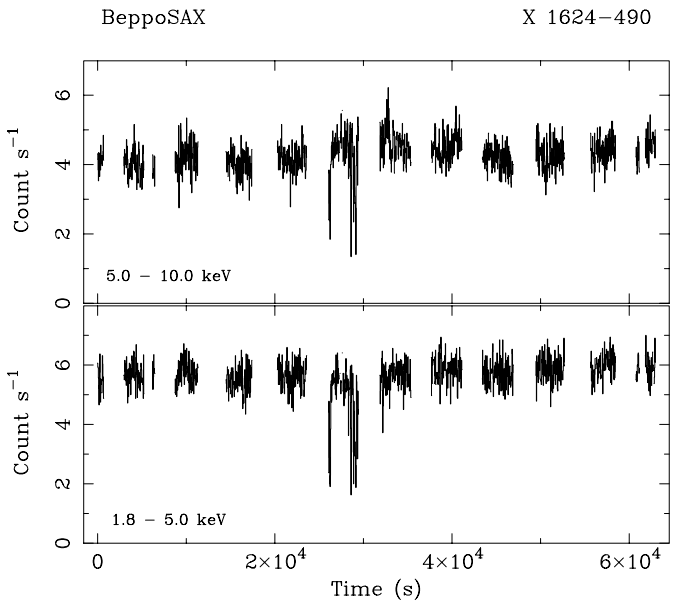

Fig. 1. MECS light curves of X 1624-490 in two energy bands: 1.8–5.0 and 5.0–10.0 keV with 32 s binning

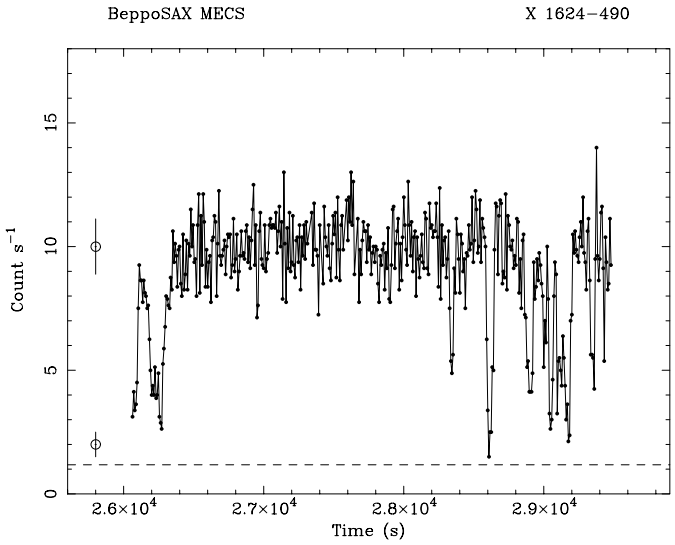

Fig. 2. Expanded view of the light curve in the energy range 1.8–10 keV with 8s binning. For clarity, Poisson errors are not shown on every point but are indicated separately for two intensity levels. The dotted line shows the expected contribution in this band of the dust-scattered halo from our radial modelling (Sect. 3.3)

and PDS lightcurves due to the comparatively reduced signal-to-noise ratio in these instruments and the energy dependence of the dipping.

It can be seen from Fig. 1 having 32 s binning that dipping is not 100% deep in either energy band unlike, for example, XB 1916-053 in which dipping often reaches 100% depth at all energies below 10 keV (Church et al. 1997). However, because of the fast dip ingress and egress times, 32 s binning is not short enough to reveal the true depth. Tests showed that 8 s binning was adequately short, in which case the depth of deepest

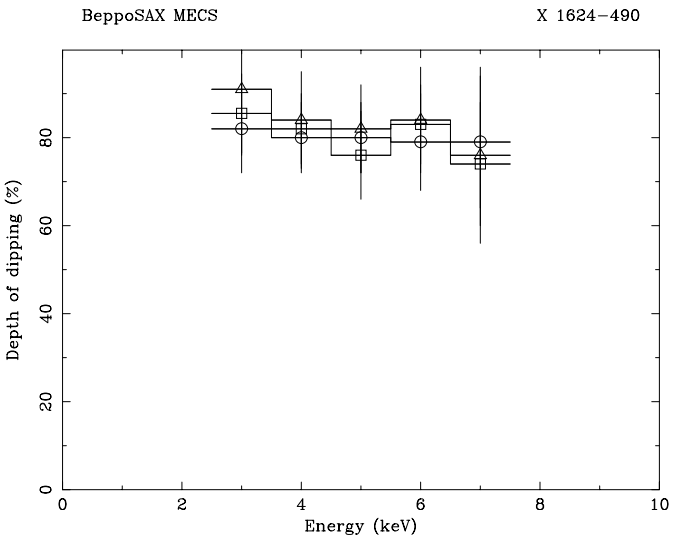

Fig. 3. Depth of dipping in X 1624-490 in several energy bands in the energy range 2–10 kev from MECS data for data extraction from 15′ radius (squares), 4′ radius (circles) and 2′ radius (triangles)

dipping was $83 \pm 5\%$ and $78 \pm 5\%$ in the bands 1.8–5.0 keV and 5.0–10.0 keV respectively. In Fig. 3 we show the results of determining the depth of dipping in the energy bands 2.5–3.5 keV, 3.5–4.5 keV, 4.5–5.5 keV, 5.5–6.5 keV and 6.5–7.5 keV from MECS data with 8 s binning. Results are shown for data extracted in the standard radius of 4′ and also for extraction radii of 2′ and 15′. For 15′ extraction, it was necessary to subtract background to avoid errors in the depth. It was not possible to obtain results outside the overall band of 2.5–7.5 keV because of poor statistics. Although there is no dramatic change in depth with energy, there is evidence for the depth increasing at low energies, particularly for 2′ extraction with 90% deep dipping at 2.5–3.5 keV. There is also evidence that dipping was deeper with 2′ extraction, but no evidence for differences between 4′ and 15′ extraction.

Thus dipping is $\sim$ 80% deep over much of the 1–10 keV band, but is not actually proven to be 100% at any energy. There can be two reasons for this. Because the Galactic column density in X 1624-490 appears to be high, dust scattering is expected to be important and below 5 keV this can result in a non-zero intensity level in deepest dipping. Above $\sim$5 keV, dust scattering will not be important, and non-zero dip intensity can be due to incomplete absorption of one emission component. The increase in depth of dipping in 2′ extraction is consistent with a decreased amount of dust-scattered halo. The column density of X 1624-490 from spectral fitting is high and so we have investigated possible effects of dust scattering. This is discussed in detail in Sect. 3.3.

3.2. The orbital period

We cannot carry out folding analysis of the present *BeppoSAX* X-ray light curve to determine the orbital period; however, we have examined the *RXTE* ASM data on this source to determine

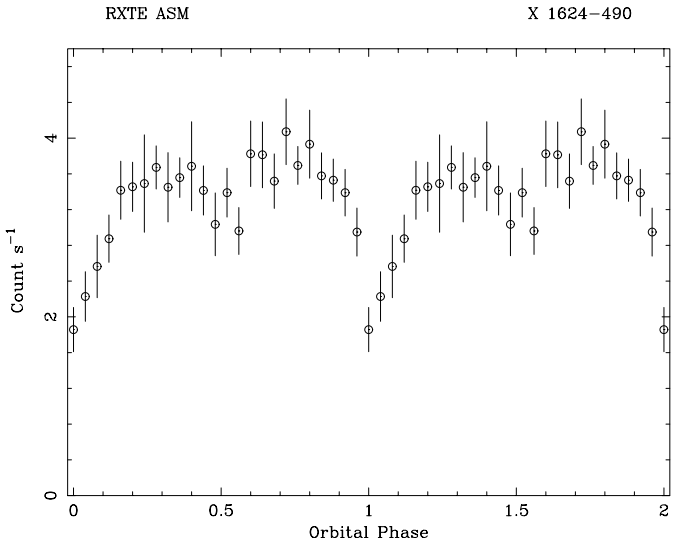

Fig. 4. Folded light curve of *RXTE* ASM data produced from 32 days of data folded on a period of 20.87 hr

the period more accurately which previously was only poorly known at 21±2 hr (Watson et al. 1985). Data were used between 1996, Feb. 20 and 2000, Jan. 18 and a period search carried out using standard (XRONOS) power spectrum software spanning the period range 2.5 – 4×10^4 hr. Peaks were seen with high significance corresponding to periods of 20.87 ± 0.01 hr and 10.438 ± 0.001 hr, the significance of each of these peaks corresponding to a probability $>>$ 99.8% of being real. 32 days of data folded on the period of 20.87 hr are shown in Fig. 4, in which dipping is clearly seen to repeat at 20.87 hr with interdipping also seen between the main dips. This is the first detection of interdipping in this source. In the four years of ASM data analysed, the depth of dipping investigated in 32 day sections of data varies, and in particular, the depth of interdipping varies from being as deep as the main dipping to being undetectable. There is some evidence that this pattern repeats on a timescale of ∼70 days, but this cannot yet be identified definitely as a new periodicity in the system. The 10.438 hr periodicity cannot be the orbital period for several reasons: firstly this periodicity is at times not present in the ASM data when the 20.87 hr periodicity is present. Additionally, Fig. 4 shows dipping at 10 hr from the main dips is weak, entirely consistent with interdipping. If the orbital period were 10.438 hr, then a strong peak at 21 hr would not be seen in the power spectrum. Finally, the *Exosat* ME lightcurve (Jones & Watson 1989; Church & Bałucińska-Church 1995) allows the possibility of a 10-hr orbital period to be almost certainly rejected.

3.3. The dust scattering halo

Although the column density of X 1624-490 is high ($\sim 9 \times 10^{22}$ atom cm^{-2} in the present work), implying that dust scattering effects will be important, radio measurements have indicated a lower value of $\sim 2 \times 10^{22}$ atom cm^{-2} (Dickey & Lockman 1990; Stark et al. 1992) (although these measurements may underestimate $\mathrm{N_H}$ when this is high), so that there is a possibility that the high value of $\mathrm{N_H}$ is due to absorption intrinsic to the source. To investigate dust scattering, we have carried out modelling of the radial intensity distribution. This was done using MECS data since spectral evolution during dipping was investigated primarily with MECS. The modelling was based on the technique used by Predehl & Schmitt (1995; hereafter PS95) in their investigation of 25 Galactic sources (not including X 1624-490) subject to high Galactic column densities using the *Rosat* PSPC. In the case of X 1624-490 we find excesses in the radial profile above the point spread function (PSF) of the instrument for radii greater than ∼100″ indicating a substantial halo contribution. Software has been developed to allow fitting the radial distribution including the source contribution convolved with the PSF, a dust-scattered halo calculated on the basis of Rayleigh-Gans scattering theory with its associated radial distribution function (Predehl & Klose 1996; PS95), plus a background contribution. As the source lies in the Galactic Plane, the standard background files are not applicable, and we adopted the same approach as PS95 and allowed the background to be a free parameter. A more complete treatment would also convolve the halo with the energy-dependent PSF. However, we investigated the effect of this and found that the value of the optical depth to dust scattering would only be reduced by up to 20%. The point spread function of Boella et al. (1997) was utilised and XIMAGE used to provide a radial distribution function of the data. From the best fit of the model to the data, the halo intensity fraction f_h was derived, where f_h is defined as the fraction of the observed intensity due to the halo, and may be written in terms of the observed source intensity $\mathrm{I_x}$ and the observed halo intensity $\mathrm{I_h}$ as

$$\mathrm{f_h} = \mathrm{I_h}/(\mathrm{I_x} + \mathrm{I_h}).$$

These procedures were tested by applying them to the bright Z-track source GX 17+2 which has been observed both with *Rosat* and *BeppoSAX*. Firstly, we modelled the PSPC data on GX 17+2 and derived results similar to those of PS95. Next, we modelled the *BeppoSAX* MECS data on this source. In the case of GX 17+2 only, PS95 obtained halo fractions in 7 energy bands within the overall PSPC band, which has allowed us to compare MECS results with their results at an energy where the MECS and the PSPC bands overlap. In the band 1.7–2.1 keV a good fit was obtained with a χ^2/dof of 78/74, and a halo intensity fraction at 1.9 keV of 27 ± 2%, compared with the value of 26% which we obtain from Fig. 8 of PS95 at this energy. This good agreement gives us confidence that the modelling was correct, and that reliable values of f_h can be obtained using *BeppoSAX*. Next, modelling was carried out for X 1624-490. Initially the MECS data were binned to a minimum of 20 counts per radial bin, then further grouping was applied with radial bins grouped together in pairs to reduce fluctuations. Systematic errors of 10% were added between 10–100″ where the PSF is uncertain by about this amount, and 2% between 100-1000″ to account for uncertainties in the PSF, faint, barely resolved sources in the field of view, and other effects. Radial bins between 500–700″ were ignored where a detector support structure causes an artificial reduction

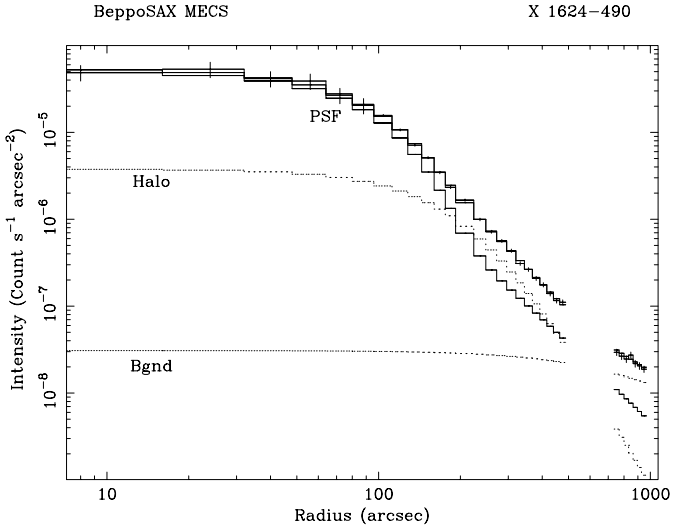

Fig. 5. Radial fitting to the MECS radial intensity distribution in the energy band 2.5–3.5 keV. The data points, the best-fit total model, the X-ray source component (convolved with the PSF), the halo component and the background contribution are shown separately

in the radial profile. The fitting was done in four energy bands: 2.5–3.5, 3.5–4.5, 4.5–5.5 and 5.5–6.5 keV. The best-fit solution is shown in Fig. 5 for the lowest band 2.5–3.5 keV in which the halo was strongest. Values of the halo fraction f_h from the best-fit models were found to be: $30 \pm 4\%$, $20 \pm 4\%$, $5.7 \pm 2\%$ in the three lowest energy bands. In the band 5.5–6.5 keV, there was no evidence for any departure of the radial profile from the PSF, and no improvement in the quality of fit by including a halo term in the model. We also calculated the halo fractions of the total count from these fitting results by integrating to a restricted outer radius of 4′, the extraction radius used for MECS spectra (Sect. 3.4). The fractions became: $26 \pm 4\%$, $19 \pm 4\%$, $5.7 \pm 2\%$ and $< 2\%$ respectively, in the four bands. When these fractions are compared with the depth of dipping in these bands (Fig. 3), it can be seen that the halo cannot explain the fact that dipping does not reach a depth of 100%, particularly at the higher energies. As discussed in Sect. 3.5, this must be due to incomplete absorption of an extended emission component. In Fig. 2 we compare the halo contribution to the intensity (dashed line) calculated from our results for the band 1.8–10 keV with the depth of dipping.

Using this limited number of energy bands, we have compared the energy variation with theoretical expectations, and derived the optical depth to dust scattering τ, evaluated at 1 keV. The reduction in source intensity is given by $\mathrm{I_x} = \mathrm{I_0}\ \mathrm{e}^{-\tau}$, from which it can be shown that the halo fraction and τ are related *via* $\mathrm{f_h} = 1 - \mathrm{e}^{-\tau}$, provided that the intensity scattered out of the line-of-sight is balanced by that scattered into the line-of-sight as is normally assumed (e.g. Martin 1970). Since the dust scattering cross-section is expected theoretically to vary as E^{-2} (Mauche & Gorenstein 1986), then the optical depth will also have this dependence, and

$$\mathrm{f_h} = 1 - \mathrm{e}^{-\tau_1\ \mathrm{E}^{-2}}$$

where τ_1 is the optical depth at 1 keV, normally quoted. Using this relation, we have derived a value at 1 keV of $\tau = 2.4 \pm 0.4$. Within the errors on the individual values of f_h, the data are consistent with an E^{-2} dependence of the cross-section.

The results show that dust scattering in the case of X 1624-490 is large. Furthermore, we can compare the above value of τ with values in Fig. 7 of PS95, in which τ is plotted against the X-ray column density for the 25 Galactic sources in this survey, and varies between zero and $\sim$1.5. Thus in X 1624-490, τ is much larger. The value of τ we obtain, and the value of $\mathrm{N_H}$ from spectral fitting of 8.6×10^{22} atom cm^{-2} may be compared with the linear τ–$\mathrm{N_H}$ relation obtained by PS95. This best relation: $\tau = 0.5\,\mathrm{N_H}\,[10^{22}] - 0.083$ predicts in our case (τ = 2.4) that $\mathrm{N_H} = 5.0 \times 10^{22}$ atom cm^{-2}, compared with our fitting result of 8.6×10^{22} atom cm^{-2} for the non-dip spectrum. The difference between these may imply a flattening of the relation at higher column density, or possibly intrinsic absorption in the source.

3.4. X-ray spectra

It has been shown that a substantial dust scattering halo is observed in X-rays around X 1624-490, and we now consider prior to presenting spectral fitting results how spectra will be affected. In the case of non-dip spectra, the effect is, in fact, expected to be zero (provided all of the halo is collected), since radiation removed from the line-of-sight is replaced by that scattered into the line-of-sight by scattering, both effects taking place predominantly at lower energies, so that the net effect on the non-dip spectrum is zero. The consequence of this is that the observed intensities due to halo: $\mathrm{I_h}$ and due to the source $\mathrm{I_x}$ are equal to the source intensity that would have been observed without scattering; i.e.

$$\mathrm{I_0} = \mathrm{I_x} + \mathrm{I_h}$$

Consequently, we did not include a dust scattering term in fitting the non-dip spectra. However, in dipping, the intensity lost by dust scattering is proportional to the dip source intensity while the intensity gained depends on the non-dip intensity because of the time delays in scattered radiation compared with unscattered. Thus, in dip data there will be an additional dust scattered component. We have carried out spectral fitting of the MECS dip spectra firstly without any additional component, and then secondly adding terms to account for the effects of dust scattering both out of and into the line-of-sight. The total halo contains both blackbody and cut-off power law terms from the spectrum incident to scattering.

The spectrum of non-dip emission was investigated by simultaneously fitting data from all the *BeppoSAX* NFI. Non-dip MECS data were selected by choosing a narrow intensity band from 9.7–10.3 count s^{-1}, also removing the dip data by time filtering. LECS, HPGSPC and PDS data corresponding to these MECS data were selected. Spectral evolution in dipping was investigated using MECS data only since the dips are not strongly seen at higher energies and there are too few counts in the LECS to contribute meaningfully. For non-dip data, the LECS and MECS spectra were rebinned to oversample the full

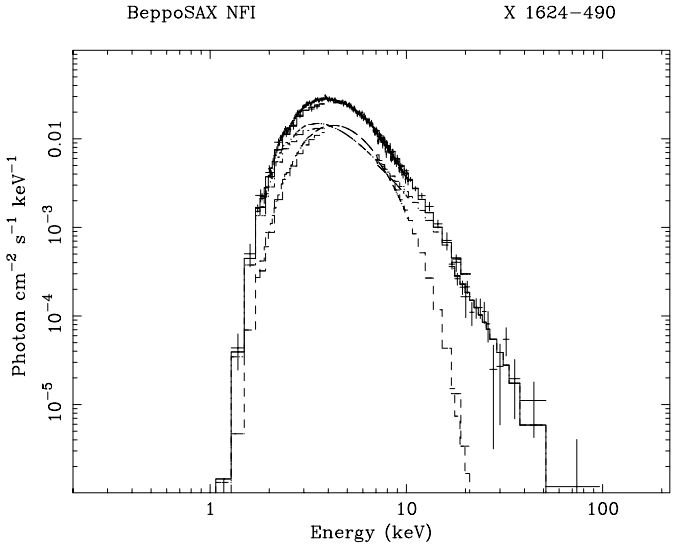

Fig. 6. The non-dip NFI X 1624-490 spectrum fitted with the absorbed cut-off power law and blackbody model discussed in the text. The total model and the contributions of the blackbody and cut-off power law components are shown separately

width at half maximum of the energy resolution by a factor of 3, and additionally LECS data were rebinned to a minimum of 20 counts per bin and MECS data to 40 counts per bin to allow use of the χ^2 statistic. The LECS and MECS non-dip spectra were also more heavily grouped to a minimum of 100 counts per bin in each case, as experience has shown that more stable fitting may result. However, in this case, results obtained with the alternative groupings were in excellent agreement. LECS data were only used between 1–4 keV and MECS data between 1.7–10.0 keV where the instrument responses are well determined. The HPGSPC data were rebinned using standard binnings in the bands 7–34 keV and PDS data were grouped appropriately for this source in which the data decrease rapidly with energy. PDS data outside the band 150–220 keV were ignored. In the following, the photoelectric absorption cross sections of Morrison & McCammon (1983) were used incorporating the Solar abundances of Anders & Grevesse (1989).

Initially, the non-dip spectrum was fitted with simple models, including absorbed power-law, thermal bremsstrahlung, blackbody and cut-off power law models. Factors were included in the spectral fitting to allow for normalization uncertainties between the instruments. Results are shown in Table 1. The power-law model was completely incapable of fitting the broad-band spectrum producing a χ^2/dof of 867/297; this was only achieved at the expense of a PDS normalization factor of 0.28 relative to MECS which cannot be real and strong discrepancies between model and data in the PDS band due to down-curving in the spectrum. The bremsstrahlung model similarly did not provide an acceptable fit with a χ^2/dof of 402/296. An absorbed blackbody model gave a fit with χ^2/dof of 651/297, the spectrum being much broader than any simple blackbody. An absorbed multi-temperature disk blackbody similarly could not fit, the model falling below the data above 10 keV. An absorbed cut-off power law model also gave a poor fit with a χ^2/dof of 396/296 and a low value of the Comptonization cut-off energy of 2.9 ± 0.3 keV which is not consistent with the spectrum extending to high energies as observed. A two-component model consisting of a disk blackbody plus a cut-off power law gave χ^2/dof almost as good as the best model (below) but with unphysical power law index and an inner radius for the disk blackbody of $\sim$0.4 km which is also unphysical.

We next tried the two-component model used extensively to fit other members of the dipping class (see Sect. 1), in which the emission regions are point-like blackbody from the neutron star and extended Comptonized emission from the ADC. This model gave an acceptable fit with a χ^2/dof of 287/294. The unfolded spectrum of this best-fit model is shown in Fig. 6. The values of the normalization factors for the individual instruments (relative to the MECS) were similar to those found for other sources.

3.5. Spectral evolution in dipping

After initial trials, MECS dip spectra were extracted with count rates between 2.0–4.0 count s^{-1}, 4.0–6.0 count s^{-1} and 6.0–8.0 count s^{-1} after first binning the data in 8 s intervals. Additionally, a spectrum was initially selected with 8.0–9.0 count s^{-1}, but this lay too close to the non-dip spectrum for parameters to be well-determined as is often found. Given the count rate of the source, a larger number of dip spectra would not be sensible. Tests showed that in this source, in which there is fast variability during dipping, binning the data into bins longer than 8 s before spectra were extracted resulted in unacceptable averaging with the consequence that the depth of dipping can appear less than it actually is. An acceptable spectral model must be able to fit both non-dip and all dip spectra, without any changes in the parameters that characterize the source emission such as blackbody temperature or power law index. In the case of weak sources, it may be necessary to fit non-dip and dip spectra simultaneously, however in X 1624-490 good fits were obtained by applying the non-dip solution to the dip spectra and using the Progressive Covering model. This model was firstly applied without any additional halo component. In this model, the emission components of the best non-dip fit are progressively covered by absorber, i.e. the extended Comptonized emission is progressively covered and the point-like blackbody is rapidly removed when the envelope of the absorber overlaps the blackbody. The model flux may be written:

$$\mathrm{e}^{-\sigma_{\mathrm{MM}}\mathrm{N_H}}\,(\mathrm{I_{BB}}\mathrm{e}^{-\sigma_{\mathrm{MM}}\mathrm{N_H^{BB}}} + \mathrm{I_{CPL}}\,(\mathrm{f}\,\mathrm{e}^{-\sigma_{\mathrm{MM}}\mathrm{N_H^{CPL}}} + (1-\mathrm{f}))$$

Good fits were obtained for all levels of dipping with this model as shown in Table 2a. It can be seen however, that the covering fraction does not rise above 50% which is inconsistent with other sources in which the progressive covering fraction rises to 100%, e.g. XB 1916-053 and XBT 0748-676 (Church et al. 1997, 1998a,b).

Next, we repeated this dip fitting with dust scattering terms added to the above best-fit models, so that

$$\mathrm{I} = \mathrm{I_d}\,\mathrm{e}^{-\tau} + \mathrm{I_n}\,(1 - \mathrm{e}^{-\tau})$$

Table 1. Spectral fitting results obtained by fitting the *BeppoSAX* NFI non-dip spectrum. N_H is in units of 10^{22} atom cm^{-2} and 90% confidence limits are given

Model	N_H	kT (keV)	Γ	E_{co} (keV)	χ^2/dof
Power law	12.87 ± 0.2	...	2.89 ± 0.04	...	867/297
Bremsstrahlung	9.9 ± 0.2	4.73 ± 0.12	...	...	402/296
Blackbody	5.5 ± 0.1	1.41 ± 0.01	...	...	651/297
Disk blackbody	8.0 ± 0.1	2.05 ± 0.03	...	...	390/297
Cutoff power-law	8.6 ± 0.4	...	0.46 ± 0.21	2.9 ± 0.3	396/296
Disk blackbody + cut-off power law	7.2 ± 0.6	5.1 ± 1.3	-0.78 ± 0.57	1.7 ± 0.3	291/294
Blackbody + cut-off power law	8.6 ± 1.0	1.31 ± 0.07	$2.0^{+0.5}_{-0.8}$	12^{+14}_{-5}	287/294

Table 2. Best fits to the dip spectra. N_H is in units of 10^{22} atom cm^{-2} for both the spectral components. 90% confidence limits are given

Spectrum	MECS ct rate (s^{-1})	N_H^{BB}	N_H^{CPL}	f	χ^2/dof
(a) without halo components					
Non-dip	9.7–10.3	8.6±0.4	8.6±0.4	0.0	150/151
Shallow dip	6.0–8.0	27±7	25±14	∼0.085	37/28
Medium dip	4.0–6.0	52±17	50±30	$0.317^{+0.047}_{-0.091}$	24/27
Deep dip	2.0–4.0	94±20	63^{+80}_{-25}	$0.492^{+0.119}_{-0.064}$	2/7
(b) with halo components					
Non-dip	9.7–10.3	8.6±0.4	8.6±0.4	0.0	151/152
Shallow dip	6.0–8.0	25±10	21^{+43}_{-12}	0.355±0.205	38/28
Medium dip	4.0–6.0	45±18	40^{+44}_{-20}	$0.607^{+0.165}_{-0.089}$	23/27
Deep dip	2.0–4.0	100^{+135}_{-20}	40^{+5}_{-19}	$0.817^{+0.003}_{-0.295}$	2/7

where I_d is the source dip intensity and I_n is the non-dip intensity. The non-dip intensity consists simply of a blackbody plus a cut-off power law with Galactic absorption, and I_d is given by the equation above in which these emission components are subjected to Progressive Covering. The net model can be expressed in the simplified form: $\mathrm{AG}\,e^{-\tau}(\mathrm{AB.BB} + \mathrm{PCF.CPL}) + \mathrm{AG}(1 - e^{-\tau})(\mathrm{BB} + \mathrm{CPL})$ where AG represents Galactic absorption, BB is the blackbody with absorption AB, CPL the cut-off power law and PCF the progressive covering fraction. Thus, the dip intensity is reduced by the cumulative effect of dust scattering and photoelectric absorption at every level of dipping, whereas the intensity scattered towards the observer is constant depending only on the non-dip source level. The optical depth was set to the best value of 2.4 obtained from the radial fitting, and the energy dependence of τ set to E^{-2}. Good fits were obtained to the non-dip and dip MECS spectra and the results are shown in Table 2b and Fig. 7. Although there is no significant improvement in χ^2/dof compared with the model without dust scattering, the results including the effects of dust scattering are clearly preferable. It can be seen from Table 2b that the progressive covering factor rises to 82% in the deep dip spectrum (2.0–4.0 count s^{-1}), i.e. still not reaching 100% which must be due to incomplete absorption of the emission components.

In Fig. 7 the fits to the non-dip and 3 levels of dipping are shown, with the evolution of the blackbody and cut-off power law components shown separately. In the top left panel the total model including all components is shown together with the total halo component itself containing blackbody and cut-off power law contributions from the incident spectrum to scattering. Firstly, it can be seen that the blackbody emission (lower right) is rapidly absorbed when the point-source becomes covered by the absorber, and is close to zero flux in the deep dip spectrum. The cut-off power law clearly displays progressive covering in that, in each spectrum, part of the spectrum at low energies is clearly unabsorbed corresponding to the uncovered part of an extended source, i.e. the accretion disk corona. The contribution of this unabsorbed part decreases as dipping deepens. In non-dip and shallow dipping this uncovered component dominates the spectrum below 5 keV. In medium dipping it is about equal to the halo contribution (at ∼3 keV), and in deep dipping the halo is larger than the uncovered emission below about 4.5 keV. However, in addition to emission uncovered by the absorber envelope, the blobbiness of the absorber demonstrated by the fast variability in dipping will also prevent dipping reaching 100%. Between the blobs, a fraction of the Comptonized emission from the ADC will be transmitted.

These results are consistent with the results obtained from *Exosat* by CBC95, who found in dipping there was strong absorption of the blackbody with weaker absorption of the Comptonized emission. Having available a set of dip spectra in the present work, not just one dip spectrum, the existence of the unabsorbed emission is revealed and the fact that progressive covering takes place.

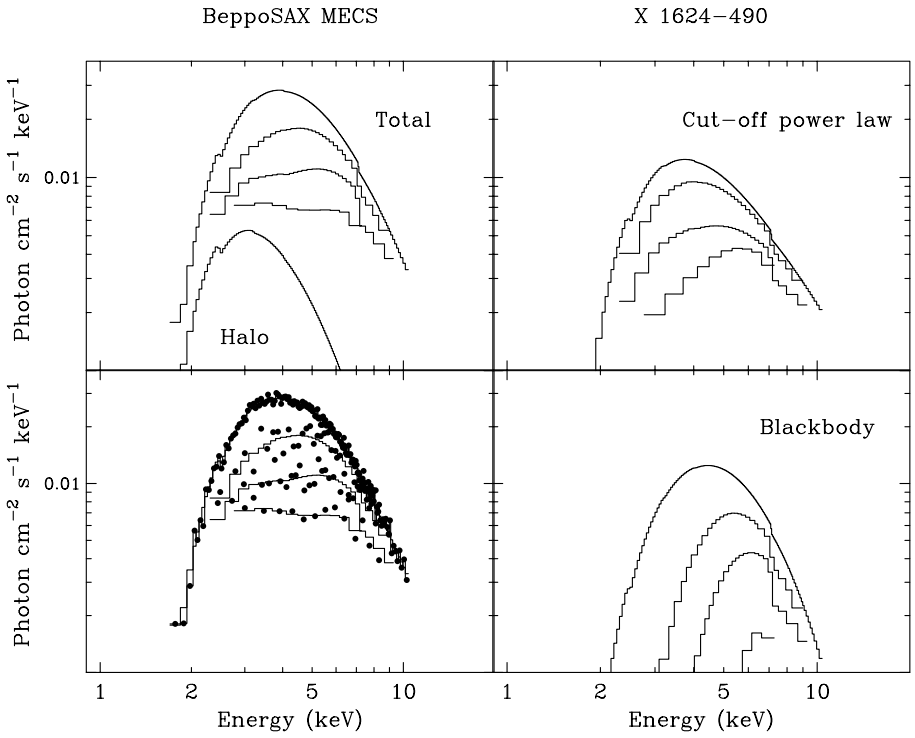

Fig. 7. Best-fit spectral fitting results to MECS non-dip and three dip spectra. Lower panel (left) shows the data and total model; lower right shows the blackbody; upper right shows the Comptonized component subject to Progressive Covering; upper left shows the total model and also the constant halo component (see text)

4. Discussion

We have shown that spectral evolution in dipping in X 1624-490 is well-described by Progressive Covering of a two-component model which assumes that X-ray emission consists of point-like blackbody emission from the neutron star plus extended Comptonized emission from an ADC. The 1–30 keV luminosity of the source is 7.3×10^{37} erg s^{-1}, for a distance of 15±5 kpc (Christian & Swank 1997), a substantial fraction of the Eddington limit, and the source is the most luminous of the dipping LMXB.

The bolometric blackbody luminosity is 2.59×10^{37} erg s^{-1}, corresponding to a blackbody radius R_{BB} of 8.3 km. If it is assumed that the emission region is an equatorial region on the neutron star in the plane of the accretion disk (a sphere intersected by two planes), the half-height of the region *h* calculated using the expression $4\pi R_{BB}^2 = 4\pi R_x h$, where R_x is the radius of the neutron star (assumed to be 10 km), is 6.8±1.8 km. Thus the blackbody emission is from a large fraction of the stellar surface. The half-height *H* of the radiatively-supported inner disk calculated from the luminosity of the source is 6.3±2.9 km, in agreement with the half-height of the emission region. These results were included in a larger sample of 14 LMXB investigated using *ASCA* and *BeppoSAX* (Church & Bałucińska-Church 2000), in which approximate agreement is found between *h* and *H* over more than 3 decades in either parameter. This provides strong evidence that the neutron star and not the accretion disk is the source of blackbody emission in LMXB. Our spectral fitting supports the point-like nature of the blackbody emission and the extended nature of the Comptonized emission. The source joins the group of other dipping sources having an unabsorbed component in dipping which are well described by this combination of emission model with a progressive covering absorption model (Church et al. 1997, 1998a,b; Bałucińska-Church et al. 1999). The only sources not tested with this model were X 1746-371 and XB 1254-690, but it has been shown that *ASCA* data on these two sources are well fitted by the model (Church et al. in preparation). It thus appears that *all* of the dipping LMXB may be explained by this combination of emission model and description of covering during dips.

X 1624-490 is complicated by the dust-scattered halo. Adding halo terms to the spectral model for dip spectra showed that the covering fraction for the extended hard emission rose to ∼82% while modelling without the halo gave a maximum fraction less than 50%. Spectral modelling with halo terms also showed that in shallow and medium dipping the unabsorbed Comptonized emission dominates the low energy spectrum, but in deeper dipping the halo becomes dominant at low energies. In the deepest dip spectrum, the halo exceeds the uncovered Comptonized emission below 4.5 keV. Angelini et al. (1997) in an analysis of *ASCA* data also used the X-ray image to estimate the extent of the halo, and suggested that the halo could explain the soft excess in dip spectra. The present work shows that the halo dominates in deepest dipping, but in less deep dipping the uncovered Comptonized emission of the ADC is the major origin of the soft excess.

We have modelled the radial intensity distribution function in several energy bands to obtain the halo fraction in these bands, and also the optical depth to dust scattering at 1 keV which was found to be τ = 2.4±0.4. This value is larger than for any of the sources studied by Predehl & Schmitt (PS95), and the halo has appreciable effect on the the dip spectra. It is not sensible to

regard dust parameters obtained from the modelling as providing definitive information on interstellar dust, since the radial modelling does not depend sensitively on the dust model used.

Dipping allows us to estimate the size of the ADC from dip ingress times. The fast variability on timescales of $\sim$32 s is clearly associated with individual blobs of absorber covering the point-source blackbody and so is unrelated to the size of the ADC. However, other observations of the source have consistently shown extended, relatively shallow shoulders to the deep dipping which we can identify with the extended emission region being progressively covered by the absorber. This is just detectable in Fig. 1. Using the *Exosat* observation and the *RXTE* observation of Sept. 1999 (Smale et al. in preparation), we estimate an average ingress time for this slow modulation of 12500$\pm$2000 s. The dip (shoulder) ingress time Δt is the time taken for the bulge in the outer disk to cross the diameter of the X-ray emitting ADC, and is obtained via the velocity of the outer disk given by

$$2\,\pi\,\mathrm{r_{disk}}/\mathrm{P}\;=\;\mathrm{d_{ADC}}/\Delta\mathrm{t},$$

where *P* is the orbital period. Using a period of 20.87 hr and a mass of the neutron star of 1.4$\mathrm{M}_{\odot}$ we derive an accretion disk radius (Frank et al. 1987) of 1.0×10^{11} cm and thus a radius of the ADC of 5.3×10^{10} cm. It is remarkable that in the case of this source, the ADC extends to $\sim$50% of the accretion disk radius, compared with $\sim$10% in XB 1916-053 and XB 1323-619 (Church et al. 1998b; Bałucińska-Church et al. 1999). However, given that the luminosity is $\gtrsim 10$ times higher in X 1624-490 it is not surprising that the ADC, probably formed by evaporation by the central source and the ADC itself, extends to much larger radii.

In summary, we have completed an X-ray study of X 1624-490 using *BeppoSAX*. We have obtained an improved orbital period of 20.87 ± 0.01 hr and made the first discovery of interdipping. We have investigated the depth of dipping in several energy bands and carried out modelling of the radial intensity distribution to obtain the halo fraction at several energies. From these data, the optical depth to scattering was derived, and an approximate E^{-2} dependence of the optical depth confirmed. Spectral fitting results for the broadband non-dip spectrum are presented, and including a halo component in spectral fitting we have shown that spectral evolution is entirely consistent with progressive covering of blackbody emission from the neutron star and extended Comptonized emission from the ADC.

References

Anders E., Grevesse N., 1989, Geochimica et Cosmochimica Acta 53, 197

Angelini L., Parmar A.N., White N.E., 1997, In: Wickramasinghe D.T., Bicknell G.V., Ferrario L., Proc. IAU Colloquium 163, Port Douglas, 1996

Bałucińska-Church M., Church M.J., Oosterbroek T., et al., 1999, A&A 349, 495

Boella G., Chiappetti L., Conti G., et al., 1997, A&AS 122, 327

Christian D. J., Swank J. H., 1997, ApJS 109, 177

Church M.J., Bałucińska-Church M., 1995, A&A 300, 441

Church M.J., Bałucińska-Church M., 2000, ApJ, submitted

Church M.J., Dotani T., Bałucińska-Church M., et al., 1997, ApJ 491, 388

Church M.J., Bałucińska-Church M., Dotani T., Asai K., 1998a, ApJ 504, 516

Church M.J., Parmar A.N., Bałucińska-Church M., et al., 1998b, A&A 338, 556

Courvoisier T.J.-L., Parmar A.N., Peacock A., Pakull M., 1986, ApJ 309, 265

Dickey J.M., Lockman F.J., 1990, ARA&A 28, 215

Frank J., King A.R., Lasota J.-P., 1987, A&A 178, 137

Frontera F., Costa E., Dal Fiume D., et al., 1997, A&AS 122, 371

Jones M.H., Watson M.G., 1989, Proc. of 23rd ESLAB Symposium, Bologna

Manzo G., Guarrusso S., Santangelo A., et al., 1997, A&AS 122, 341

Martin P.G., 1970, MNRAS 149, 221

Mauche C.W., Gorenstein P., 1986, ApJ 302, 371

Morrison D., McCammon D., 1983, ApJ 270, 119

Parmar A.N., White N.E., Giommi P., Gottwald M., 1986, ApJ 308, 199

Parmar A.N., Martin D.D.E., Bavdaz M., et al., 1997, A&AS 122, 309

Predehl P., Klose S., 1996, A&A 306, 283

Predehl P., Schmitt J.H.M.M., 1995, A&A 293, 889 (PS95)

Smale A.P., Mukai K., Williams O.R., Jones M.H., Corbet R.H.D., 1992, ApJ 400, 330

Stark A.A., Gammie C.F., Wilson R.W., et al., 1992, ApJS 79, 77

Watson M.G., Willingale R., King A.R., Grindlay J.E., Halpern J., 1985, IAU Circ. 4051

White N.E., Swank J.H., 1982, ApJ 253, L61